The Effect of Multiwalled Carbon Nanotube Dimensions on the Morphology, Mechanical, and Electrical Properties of Melt Mixed Polypropylene-Based Composites

Irina Dubnikova,[1] Evgeniya Kuvardina,[2] Vadim Krasheninnikov,[1] Sergey Lomakin,[3] Igor Tchmutin,[4] Sergey Kuznetsov[5]

[1]*Department of Polymer and Composite Materials, N.N.Semenov Institute of Chemical Physics, Russian Academy of Sciences, Kosygin st., 4, Moscow 119991, Russia*
[2]*Department of Physics, Chemistry and Technology of Polymers, Lomonosov State Academy of Fine Chemical Technology, Vernadsky Pr., 86, Moscow 119571, Russia*
[3]*Polymer Material Science Department, N.M.Emanuel Institute of Biochemical Physics, Russian Academy of Sciences, Kosygin st., 4, Moscow 119991, Russia*
[4]*Department of Nanocomposites, Institute for Nanotechnologies of ICF, B.Tatarskaya st. 38, Moscow 115184, Russia*
[5]*Neutron Physics Department, Lebedev Physical Institute, Russian Academy of Sciences, Leninsky Pr., 53, Moscow 119991, Russia*

Received 19 August 2009; accepted 16 December 2009
DOI 10.1002/app.31979
Published online 2 March 2010 in Wiley InterScience (www.interscience.wiley.com).

ABSTRACT: The effect of multiwalled carbon nanotube (MWCNT) dimensions and surface modification on the morphology, mechanical reinforcement, and electrical properties of PP-based composites, prepared by melt mixing, has been studied. The MWCNTs of small ($d < 10$ nm) and large ($d = 40$–60 nm) diameters with various intrinsic aspect ratios (L/d) have been used as filler. Transmission electron microscopy and very cold neutrons (VCN) scattering showed that both as-received and surface modified small diameter MWCNT(1)s exhibit a strong tendency to bundle or cluster together in melt compared to both long MWCNT(3)s and short MWCNT(2)s large diameter nanotubes. The fractions of isolated nanotubes are higher and the mass-fractal dimensions are lower for thick MWCNT-based nanocomposites. The nanotubes of all types are heterogeneous nucleation sites for PP crystallization. The tensile and DMA testing results revealed that both long thick MWCNT(3)s with $L/d \approx 300$ and thin MWCNT(1)s with highest intrinsic $L/d > 1000$ exhibit similar reinforcing effects, because drastically decreasing the effective aspect ratio $(L/d)_{\text{eff}}$ of the thin flexibly nanotubes within polymer matrix. The nanocomposites based on the long large diameter MWCNT(3)s demonstrated the lowest percolation threshold equal to 1.5 vol % loading, highest dielectric and electromagnetic waves shielding properties. It was concluded that the choice of optimal diameter and length of MWCNTs is right approach to the improvement in the dispersion state and straightness of multiwelled carbon nanotubes in polymer melt as well as to enhancement of their efficiency as reinforcing and conductive nanosized filler. © 2010 Wiley Periodicals, Inc. J Appl Polym Sci 117: 259–272, 2010

Key words: nanocomposites; poly(propylene) (PP); structure–property relations; reinforcement; conducting polymers

INTRODUCTION

Since their discovery in 1991, carbon nanotubes (CNT) have generated huge activity in many areas of science and engineering due to their unprecedented physical and chemical properties.[1–6] The CNT have diameters in the nanometer scale, are up to tens of microns long, and can be single- or multi-walled (SWNT and MWNT, respectively). Owing to high aspect ratio (larger than 1000), high strength and stiffness at low density the CNTs attract attention of the researchers as reinforcing fillers for a generation of new high performance low weight structural polymer composites.[2,3] Other interesting properties of CNTs, such as the high electrical and thermal conductivity, are used to develop functional materials possessing electrical and thermal conductivity, electromagnetic absorbing or energy storage performances, heat resistance, chemical sensing, etc.[3–6] Over the last decade many polymers, such as epoxy,[7,8] PMMA,[9] PA,[10] PC,[11,12] PS,[13,14] PE[15–17] and PP,[18–21] have been employed as matrices for preparation of CNT/polymer composites. It was established that the CNT/polymer composites reveal much lower electrical percolation thresholds

Additional Supporting Information may be found in the online version of this article

Correspondence to: I. Dubnikova (ild@chph.ras.ru).

Contract grant sponsor: Russian Foundation of Fundamental Research; contract grant numbers: 09-03-12232, 06-02-39032.

compared to carbon black (CB) and carbon fiber based composites.[3–5]

To date the reported results on the CNT/polymer composite properties are scattered and still far from satisfactory.[3–5,22–25] Very diverse percolation thresholds for CNT-based composites have been reported by various research groups—from 0.0025 wt % for CNT/epoxy composites up to 11 wt % for SWNT/poly(3-octylthiophene) composites.[4] Analyses of research results show that performance of the CNT-based composites depends on many factors, such as type of CNTs (SWNTs or MWNTs), their structure (diameter, length, and bundling), processing method, choice of matrix,[25] CNT dispersion within matrix,[24] interfacial interaction between CNTs and matrix, and so on. Due to high specific surface area and high interparticle van der Waals attractions the nanotubes have a tendency to agglomerate or cluster together, resulting generally in increased difficulties in dispersing nanoparticles within the polymer matrix during processing stage. Common fabricating methods of the CNT/polymer composites include solution mixing, *in situ* polymerization and melt blending. **Solution mixing** is considered as an effective technique to overcome a nonuniform CNT distribution and is often used to prepare composites based on soluble polymers, but it is completely unsuitable for many polymer types that are insoluble. ***In situ* polymerization** is considered as a very efficient method to significantly improve the CNT dispersion and the interaction between CNTs and polymer matrix. **Melt blending** is a solvent-free versatile method and is commonly used to fabricate composite materials, especially for thermoplastic polymers. All the CNT/polymer composites based on thermoplastic polymers as matrix can be processed in this manner. However, many experimental results have shown that of all the processing methods, the overall results are worst for the melt based systems.[2–4] Most of the melt processed randomly oriented CNT/polymer composites exhibit only a moderate or no modulus enhancement.[2,3,6,23] In addition, the electrical percolation thresholds found for CNT-composites based on semicrystalline thermoplastic matrices (PP, PE, PEO, and PA) are always higher than those of the CNT/epoxy composites.[3–5,7,8]

As it was concluded by a number of authors, the dispersion of nanosized fillers in the polymer melt is more difficult than that of micron sized fillers. The major obstacles for realization of CNT technological potential are the bundling, entanglement, and waviness of CNT in polymer melt.[4,25,26] However, any nanotube reinforced composites produced at industrial level are likely to be produced by melt processing. For these reasons the main challenge is to improve the dispersion and alignment of CNTs in a polymer matrix during the melt mixing stage. One option is to optimize the nanotube dimensions. The purpose of this work was to analyze the role of such factors as nanotube diameter and length as well as surface modification on the CNT dispersion state in a polypropylene matrix and the resulting properties of the PP/CNT nanocomposites. Nowadays PP is widely used because of its good properties–cost balance, as well as its excellent processability and low density. The PP nanocomposites with MWCNTs of three dimensions were processed by melt mixing and relationships between the MWCNT dimensions, composite morphologies, mechanical reinforcement, and electrical properties were studied.

EXPERIMENTAL

Materials

Isotactic PP (Moscow Naphta Processing Plant., Russia) with a melt flow index MFI = 0.6 g/10 min (2.16 kg, 230°C) was used as a matrix polymer (M_w = × 10^5 6.3 × 10^5 g/mol, M_w/M_n = 3.5). Multiwalled carbon nanotubes (MWCNT) were supplied by Shenzhen Nanotech Port Co. (China). MWCNTs with amorphous carbon <3% were prepared by chemical vapor deposition. Three types of MWCNTs with different average diameter (d), length (L), and aspect ratio (L/d) (Table I) were investigated as nanosized filler.

Preparation of the nanocomposites

Composites were prepared by melt mixing in a two-roller mixing chamber (Brabender mixer) at 190°C and a rotor rotation speed of 60 rpm. First, PP was melt blended with stabilizers of the thermo-oxidative

TABLE I
Characteristics of Multiwalled Carbon Nanotube Used

MWCNT type	d (nm)[a]	L (μm)[a]	L/d	ρ (g/cm^3)[a]	σ_{dc} 10^{-3} (S/cm)[b]
MWCNT(1)	<10	5–15	500–1500	2	1.82 ± 0.36
MWCNT(2)	40–60	1–2	20–40	2	0.82 ± 0.16
MWCNT(3)	40–60	5–15	100–300	2	0.65 ± 0.13

[a] producer's data
[b] author's data

degradation (0.3 wt % of topanol and 0.5 wt % of dilauriltiodipropionate) for 3 min. The CNT were then added slowly for 3 min and the mixture was compounded for 15 min. Two kinds of the PP composites were prepared, based on both as-received and surface modified MWCNTs. To improve compatibility of MWCNTs and iPP and to enhance their dispersion in the PP matrix, CNT were chemically modified by grafting of aliphatic chains onto the MWCNT surface. The most well known CNT functionalization method is the strong acid oxidation of the CNTs by a concentrated acid, such as sulfuric or nitric acid or their mixture.[26–30] Our strategy for MWCNT functionalization was to use preliminary ozone treatment of MWCNTs followed by ammonolysis of epoxy groups formed on the MWCNT surface. The selective ozonization of MWCNTs was carried out with ozone–oxygen mixture (ozone concentration was 2.3×10^{-4} mol/L) in a bubble reactor. Then the ammonolysis of oxidized MWCNTs has been carried out by tert-butylamine in the ultrasonic bath (35 kHz) at 50°C for 120 min with following evaporation of tert-butylamine excess. The presence of the alkylamine groups at the MWCNT surface was confirmed by IR transmission spectroscopy as the appearance of the characteristic band $\sim$ 1210 cm^{-1} corresponding of the valence vibration of the N—C< bond (Supporting Information, Figure SI1). The resulting surface modified CNT were termed as m-MWCNTs. The nanoparticle loadings (Φ) were in the range of 0.1–5 vol % (0.2–10 wt %). For comparison, the unfilled PP was also processed in the mixer.

Specimen preparation

The specimens for morphological and mechanical testing as 0.5 mm-thick plates were compression molded. The molding procedure involves heating at 190°C for 5 min without applied pressure and then for 5 min under pressure (10 MPa). The mold was cooled to 90°C by water at a rate of 16 K/min under pressure.

Structural characterization

Transmission electron microscopy

The dispersion of the pristine MWCNT powers as well as the their dispersion state and distribution in the PP matrix were examined by transmission electron microscopy (TEM) on LEO-912 AB OMEGA (Germany) instrument using an accelerating voltage of 100 kV. Ultrathin sections of composite specimens with a thickness of about 100 nm were prepared using a Reichert–Jung Ultracut ultramicrotome with diamond knife.

Very cold neutrons scattering

To compare the effects of MWCNT size, loading, and surface modification on some average numerical structural parameters of the composite morphology, like the volume fraction of isolated MWCNTs (ν) (the ratio of isolated MWCNT volume concentration φ to the total filler volume concentration) and mass–fractal dimension (D), very cold neutron (VCN) scattering method was additionally used. Very cold neutrons can be defined as neutrons with velocities (v) about 10–100 (M/C) and energies below 10^{-2} (m/s), that corresponds to the wavelength values of $\lambda > 4.0$ nm. The most convenient scattering objects for VCN method are the nanoscale elements (NSE) with average sizes of 2.5–50 nm. The time-of-flight VCN spectrometer developed at Lebedev Physical Institute (situated at the Research reactor of Moscow Engineering Physics Institute) was used.[31] The VCN method is based on measuring the falling on the sample [$I_0(k)$] and passed through the sample [$I_1(k)$] VCN intensities:

$$I_1(k) = I_0(k) \exp\left(-\sum\nolimits_t x\right), \quad (1)$$

where x is sample thickness, k – neutron wave vector modulus, $\Sigma_t = \Sigma_a + \Sigma_{in} + \Sigma_H + \Sigma_{es}$ is the VCN total cross section (Σ_a, Σ_{in}, Σ_H, Σ_{es} are the cross sections for the absorption, inelastic scattering, incoherent nuclear scattering, and elastic scattering on NSE, respectively).

The wave vector modulus (k) dependencies of the VCN total cross section $\Sigma_t(k)$ were obtained from (1). $\Sigma_{es}(k)$ dependencies were isolated from $\Sigma_t(k)$ and the integral of neutron scattering intensity ($I_S(q)$) depending on wave vector modulus was obtained:

$$\sum\nolimits_{es}(k) = (2\pi/k^{-2}) \int_{2k\sin\theta d}^{2k} I_S(q) q dq. \quad (2)$$

q—neutron wave vector transfer, $q = 2k\sin\theta$, θ—scattering angle, θd—angular size of the VCN detector.

The theoretical dependency of the VCN elastic scattering on NSE cross section [$\Sigma_{es}(k)_{calc}$] with using two correlation functions of both hollow straight cylinder and fractal type structure was applied to describe the VCN scattering on both the isolated MWCNTs and nanotube agglomerates (Supporting Information). The volume fraction of isolated nanotubes φ and the mass-fractal dimension D were evaluated by fitting of the experimental and the theoretical $\Sigma_{es}(k)$ dependencies.

Differential scanning calorimetry

Crystallization and melting behaviors of the unfilled PP and the PP matrix in the presence of MWCNTs were investigated using a DSC-204 F1 differential

scanning calorimeter (Netzsch, Germany) under a nitrogen atmosphere. Heating and nonisothermal crystallization DSC experiments were carried out in the 25–180°C range at a rate of 10 K/min. The thermograms were used to determine the onset melting temperature, peak melting temperature (T_m) and enthalpy of melting (ΔH_m), and peak crystallization temperature (T_{cr}). The specific heat flow from the melting peak (W/g) was corrected for the mass of PP in the nanocomposite. The PP-matrix crystallinity in the nanocomposites was calculated with using the melting enthalpy value for 100% crystalline PP $\Delta H_{m100} = 209$ J/g.[32]

Mechanical properties

Tensile test

For mechanical testing, the dumbbell specimens with dimensions 30 mm × 5 mm × 0.5 mm were cut from hot pressed films. The uniaxial tensile testing of composites was carried out using a tensile testing machine (Instron-1122) with a crosshead speed of 20 mm/min (0.67 min^{-1}) at room temperature. Elastic modulus, yield stress and strain, stress and elongation at break were determined from the stress−strain diagrams. The average values were calculated from eight runs for each specimen.

Dynamic mechanical analysis

For the dynamic mechanical measurements, an analyzer DMA 242 C/1/F (Netzsch, Germany) was used. Bar shaped specimens of about 20 mm × 5 mm × 0.5 mm were cut from compression molded sheets. Experiments were performed in tensile mode at a frequency of 1 Hz. The samples were analyzed by dynamic strain amplitude of 0.2% in temperature range between −60 and +160°C with a constant heating rate of 2 K/min. The storage modulus G′, loss modulus G″, and loss factor tan δ were determined as functions of temperature.

Electrical properties

The following electrical properties were measured in this work: (i) direct current conductivity parallel to sample plane (σ_{dc}); (ii) alternating current conductivity and permittivity perpendicular to sample plane in frequency (f) range 10^{-2}–10^6 Hz (σ_{ac} and ε'_{ac}); (iii) dielectric permittivity and losses parallel to sample plane at 6 fixed frequencies in ultra-high frequency range 2.6–25 GHz (ε' and ε''). Room temperature dc-conductivity with accuracy 5% was measured by the four-probe method. Copper wire was used as electrode material, silver adhesive with conductivity 10^4 S/cm was used to decrease the contact resistance. AC-conductivity and permittivity were measured using Broadband dielectric spectrometer BDS-40 (Novocontrol). The samples for measurement of ac properties were disk shaped with diameter about 25 mm and thickness about 0.45 mm. Electrodes with diameter of 20 mm on both surfaces of the samples were attached using silver adhesive. The error of ac properties measurements was equal 2% and was determined mainly by geometry measurement accuracy. Dielectric permittivity and losses in microwave range were measured using resonant cavity method with rectangular resonator[33] with accuracy 10%. Rectangular plates with length 40 mm, thickness 0.45 mm, and width 0.5–2 mm were used as the samples.

Electromagnetic waves reflection (RD), absorption (A), and transmission (T) coefficients, as well as reflection coefficient from sample placed on metal plate (RM), were measured in frequency range 5.6–37 GHz using free space horn-antenna method[33] with accuracy 15%. The samples had the shape of plate with thickness about 0.45 mm.

RESULTS AND DISCUSSION

Morphology of PP nanocomposites

Effect of dimension and surface modification on the MWCNT dispersion into the PP matrix was studied by both the TEM and very cold neutrons scattering. Figure 1 shows typical TEM images of the composites based on both the as-received MWCNT(1)s [Fig. 1(a,b)] and surface modified m-MWCNT(1)s [Fig. 1(c)]. It can be seen that the thin long nanotubes with the average diameter $d < 10$ nm are all in tangle clusters and micron sized aggregates, while the fraction of isolated nanotubes is very low. In the composite prepared with surface modified m-MWCNT(1)s the aggregate sizes are slightly lower [Fig. 1(c)]. Therefore, TEM analysis reveals that it is difficult for long thin MWCNT(1)s to be separated from one another within the polymer matrix during mixing stage. Due to high flexibility and large surface area, long thin nanotubes can easily get entangled with one another whereupon their intrinsic high aspect ratio L/d does not wholly realize. Therefore the effective aspect ratio $(L/d)_{eff}$ of the nanotube aggregates is drastically reduced in the polymer composites compared to tabular data (Table I).

In contrast, the composites prepared with both the large diameter (d = 40–60 nm) long MWCNT(3)s and short MWCNT(2)s exhibit a more uniform distribution of both as-received and surface modified nanotubes in the polymer matrix (Figs. 2, 3). The microscopic analysis showed the similar morphologies for the composites with both the long (intrinsic aspect ratio $L/d \approx 300$) and short ($L/d \approx$ 20–40) large diameter nanotubes. TEM images of such samples

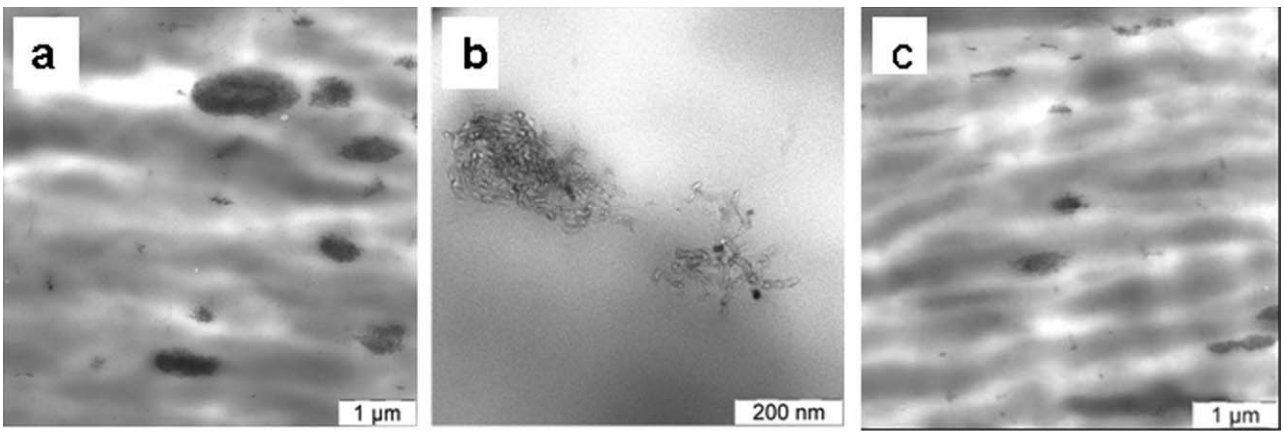

Figure 1 TEM images of PP-based composites with 3 wt % of both as-received MWCNT(1)s (a,b) and surface modified m-MWCNT(1)s (c), showing tangled aggregates of thin long nanotubes within polymer matrix.

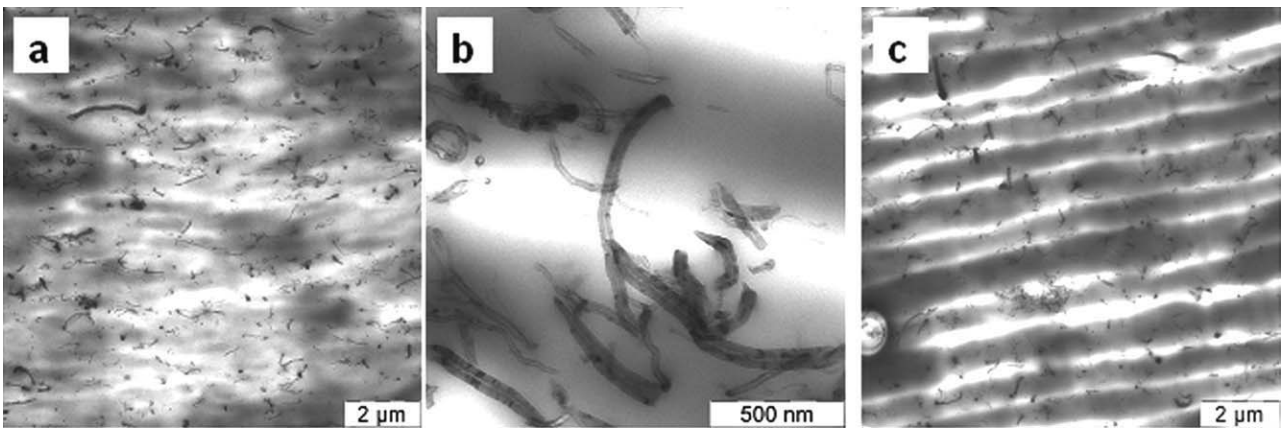

Figure 2 TEM images showing the morphology of PP composites with 5 wt % of both as-received MWCNT(3)s (a,b) and surface modified m-MWCNT(3)s (c). (b) High resolution TEM image illustrates predominantly nonentangled thick nanotubes within polymer matrix.

clearly illustrate that the thick MWCNTs mostly distributed as individual nonentangled nanotubes. Although a tendency to bundle or cluster together in melt rises slightly with increasing filler loading, sufficiently homogeneous distribution of the long as-received MWCNT(3)s throughout PP matrix was still achieved even for the composite with loading level up to 10 wt % (5 vol %). Distinctive feature of both

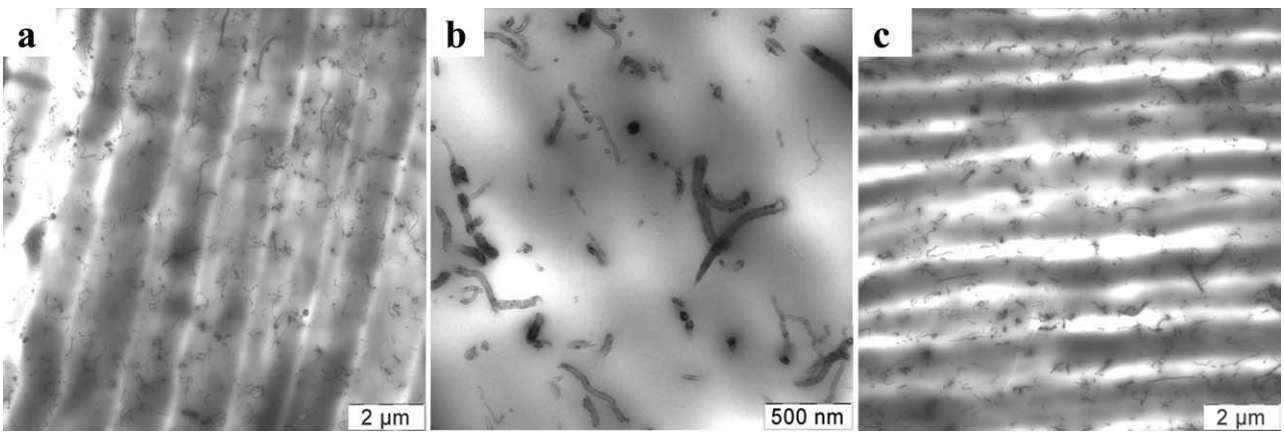

Figure 3 TEM images showing the morphology of PP composites with 5 wt % of both as-received MWCNT(2)s (a,b) and surface modified m-MWCNT(2)s (c). (b) High resolution TEM image illustrates predominantly nonentangled structure of the thick nanotubes within polymer matrix.

TABLE II
The Isolated MWCNT Fractions (ν) and Mass-fractal Dimensions (*D*) in PP Nanocomposites, Measured by VCN Scattering Method

MWCNT type	Total MWCNT volume content (Φ), vol %	MWCNT volume content measured by VCN (φ), vol %	Fraction of isolated MWCNTs (ν = φ/Φ), %	The mass-fractal dimension (adequate to cluster density) *D*
MYHT(1)	0.5	0.07	14	2.7
m-MYHT(1)	0.5	0.1	20	2.5
	1.5	0.3	20	2.5
MYHT(3)	0.5	0.3	60	1.55
	1.5	0.55	36	2.02
m-MYHT(3)	0.5	0.3	60	1.38
	1.5	0.5	33	2.02

large diameter MWCNT(3)s and MWCNT(2)s is a higher degree of the straightness within the polymer matrix compared to small diameter MWCNT(1)s, caused by higher rigidity of the thick nanotubes. Nevertheless, some degree of curving and waviness of the thick nanotubes is likewise noticeable.

The quantitative information about the dispersion state of both thin MWCNT(1)s and thick MWCNT(3)s within polymer matrix was obtained by the VCN scattering method. The data on fractions of isolated nanotubes from total introduced amount (ν = φ/Φ) and the mass-fractal dimensions (*D*) as functions of the nanotube diameter, loading, and surface modification are listed in Table II. According to the data of Table II, in the composite containing 0.5 vol % of as-received thin MWCNT(1)s the fraction of the isolated nanotubes ν was measured to be only the 14% from total introduced amount. The surface modification of the thin nanotubes results in increasing of the ν value to 20% and negligible decreasing of mass-fractal dimension. In the nanocomposites based on the thick MWCNT(3)s the measured portions of the isolated nanotubes are higher compared to those of PP/MWCNT(1) composites. At 0.5 and 1.5 vol % loadings the ν values are about 60 and 33–36 % correspondingly, independently of the nanotube surface modification. The *D* values are lower for thick MWCNT(3)-based composites. They raise from 1.4–1.5 to 2 with the increase in the MWCNT(3) loading and decrease slightly by using surface modified nanotubes.

Our experimental data, demonstrating of the decrease in tendency of MWCNTs to bundle or cluster together with increasing nanotube diameter, agree with the calculation results,[34] which suggest that the thermodynamic of mixing the CNT and polymer becomes more favorable with increasing the nanotube diameter owing to decreasing nanotube surface area.

Nucleating effect of carbon nanotubes

The effects of MWCNT dimension, loading and surface modification on the melting, and nonisothermal crystallization behaviors were analyzed by DSC. In Figure 4 the typical DSC thermograms are presented for PP/MWCNT(1) composites. In Table III the crystallization peak temperatures (T_{cr}), melting peak temperatures (T_m), and enthalpies (ΔH_m), the crystallinities are listed for neat PP and the nanocomposites with both as-received and surface modified MWCNT(1)s and MWCNT(3)s. The dependencies of

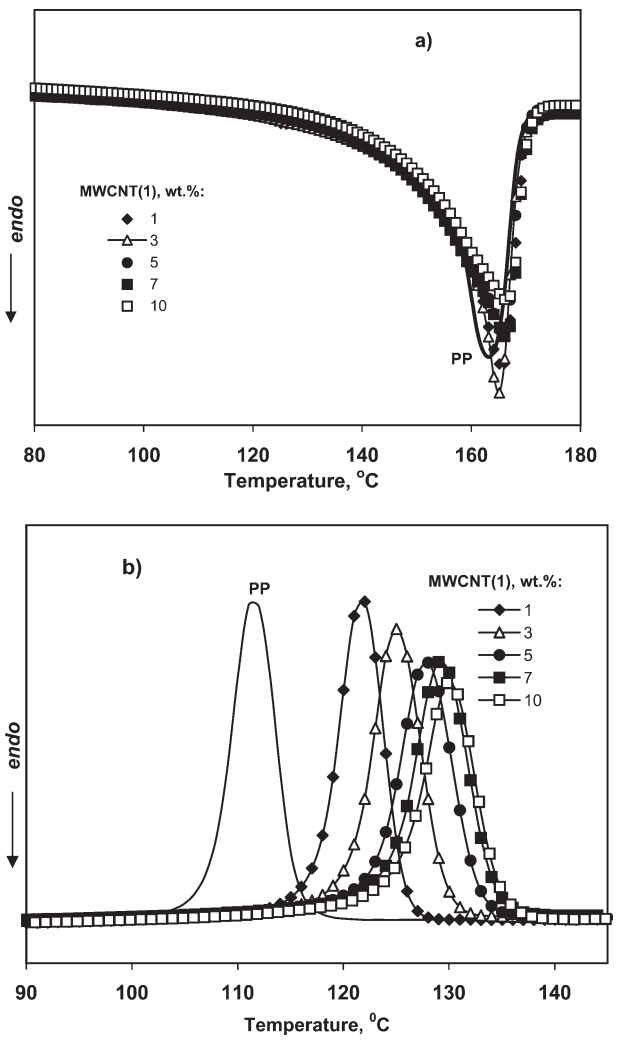

Figure 4 The melting (a) and crystallization (b) thermograms for PP/MWCNT(1) composites.

TABLE III
Calorimetric Data of Neat PP and PP/MWCNT Nanocomposites

Sample	MWCNT (wt %)	T_{cr} (°C)	T_m (°C)	ΔH_m (J/g)	Crystallinity (%)
PP	0	111.9	164.4	96.3	46
PP/MWCNT(1)	0.2	120.5	164.0	100.5	49
	1	121.4	164.8	101.0	49
	3	124	165.5	101.0	49
	5	127.8	165.9	101.0	49
	10	131	166.0	101.0	49
PP/m-MWCNT(1)	0.5	120.9	164.7	101.0	49
	1	121.7	164.5	101.0	49
	3	124.9	165.2	101.0	49
	5	127.8	166.1	101.0	49
	7	129.2	166.3	101.1	49
PP/MWCNT(3)	1	119.4	163.9	102	49
	3	121.0	162.9	98.6	47
	5	121.9	163.9	103.5	50
	7	122.6	164	99.1	47
	10	123	165.5	107	52
PP/m-MWCNT(3)	1	119.4	163.3	99.5	48
	3	121.0	164.2	100.5	48
	5	122.0	163.7	98.7	47
	6	122.1	164.5	98.8	47

the composites T_{cr} upon the nanotube loading are plotted in Figure 5. These data allow comparing the nucleating action of the different MWCNTs used during nonisothermal crystallization of PP. The increase in the T_{cr} is observed for all nanotube types, suggesting that CNTs are heterogeneous nucleation sites for PP crystallization. Interestingly, this effect is considerably more evident in the case of small diameter MWCNT(1)s. The shift in the T_{cr} is about 10°C even at the MWCNT(1) loading as low as 0.5 wt % (0.25 vol %). The reached plateau value in the MWCNT(1)-based nanocomposites exceeds that for the MWCNT(3)-based nanocomposites by more than 8°C. The observed difference in the nucleating effects of thin and thick CNTs in the course of nonisothermal crystallization of the PP results evidently from the larger specific surface of the small diameter MWCNT(1)s, in spite of their tendency to agglomeration. As can be seen from the Table III, the minor tendency to the increase in the crystallinity and T_m of PP matrix is observed with increasing nanotube loading. Probably the role of nucleating action of MWCNTs on the PP matrix morphology comes to decreasing in the PP spherulite sizes as it was reported.[35]

Nanocomposite tensile properties: reinforcement

The used pristine PP has following main mechanical characteristics: the tensile modulus $E = 1250$ MPa; yield stress $\sigma_y = 33.5$ MPa, strain at yield $\varepsilon_y = 11\%$, necking stress $\sigma_{neck} = 23.2$ MPa, tensile strength $\sigma_b = 45$ MPa and elongation at break $\varepsilon_b = 750\%$. The effects of MWCNT loading on the composite relative tensile moduli (E/E_{PP}) and yield stresses are demonstrated in Figure 6 depending on MWCNT type and surface modification. The E/E_{PP} ratio characterizes the reinforcing effect of rigid filler and normally increases with increasing particle anisotropy. From Figure 6(a), it is evident that the short thick MWCNT(2)s with lowest aspect ratio $L/d \approx 20$–40 manifest lowest reinforcing effect compared with those of both thin MWCNT(1)s and thick MWCNT(3)s with higher L/d values. On the other hand, it is worth mentioning that no significant difference was observed in the reinforcing effects of MWCNT(1)s with intrinsic $L/d > 1000$ and MWCNT(3)s with intrinsic $L/d \approx 300$, and the

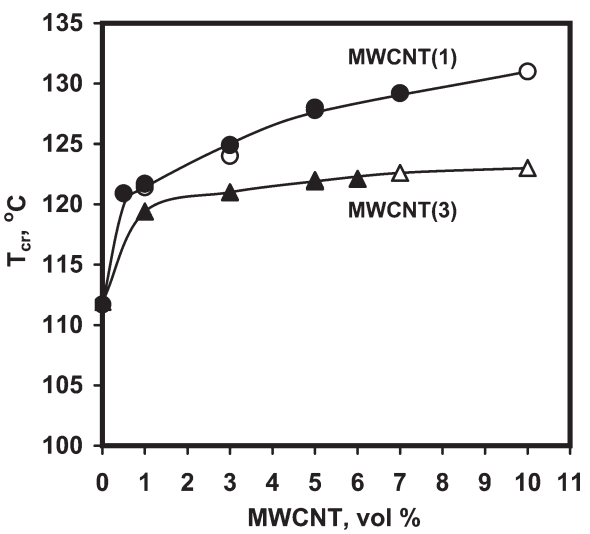

Figure 5 The dependencies of the nanocomposite crystallization temperature upon the MWCNTs volume loading for as-received (open symbols) and surface modified (closed symbols) MWCNT(1)s and MWCNT(3)s.

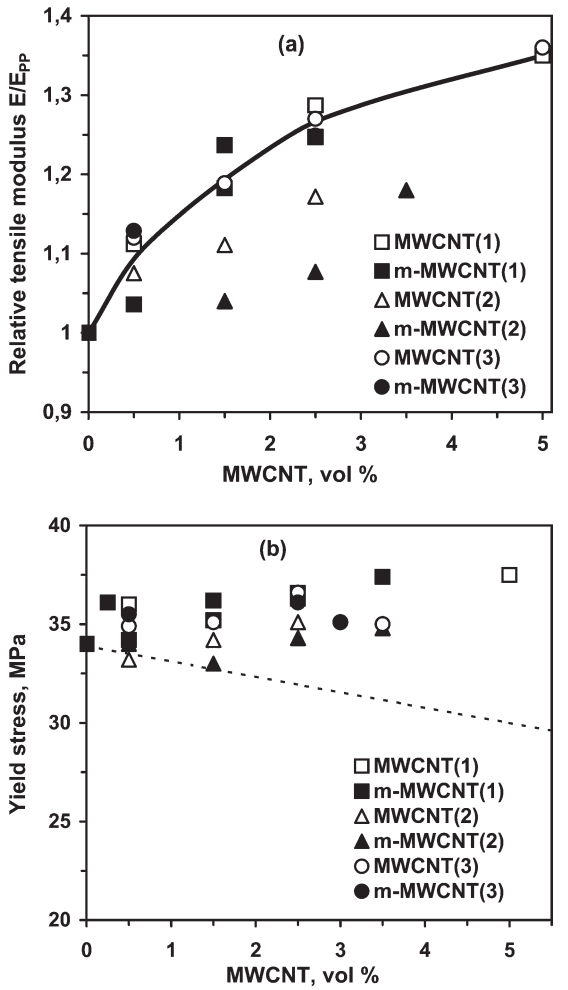

Figure 6 The relative elastic moduli E/E_{pp} (a) and yield stresses (b) of PP/MWCNT composites as functions of the nanotube volume loading depending on the nanotube type and surface modification. The solid line in (a) is fit to ultimate E/E_{pp} values. The dashed line in (b) is the concentration dependency of the σ_y calculated for composite with zero adhesion.[37]

maximal E/E_{PP} values were about 1.35–1.40 for 5 vol % nanotube loading. Such low reinforcement efficiency of MWCNT(1)s with intrinsic aspect ratio higher than 1000 is far behind the idealized theoretical predictions from the rule of mixtures and the Halpin-Tsai model,[36,37,2] based on the unidirectional alignment of anisotropic fibrous particles and perfect interfacial adhesion between the matrix and filler. From Figure 6(b), it is seen that the composite yield stress σ_y gradually rises from 33.5 MPa for unfilled PP up to 35–37 MPa for the composites with 5 vol % of nanotubes, opposed to falling dependency of the σ_y upon filler content predicted by the model for composite with zero adhesion (dashed line).[38] From these results, it is deduced that interfacial adhesion between the nanotubes and polymer matrix takes place, whereupon an efficiency of load transfer from the polymer matrix to the nanotubes during stretching increases. Most likely the wide gap between the predicted high reinforcing effect for high anisotropic rigid fibrous particle and the experimental reinforcement efficiency of MWCNT(1)s is caused by the random orientation and drastic decrease in the $(L/d)_{eff}$ of the thin flexible nanotubes, that is in agreement with our TEM data (Fig. 1).

Moreover, the addition of further 0.25 vol % of any used MWCNT type leads to a sharp drop in ductility and brittle fracture of nanocomposites. The variation in the compounding time and addition of compatibilizers (triton X-100, telomeres of fluoridize alcohols) did not lead to improving the composite toughness. Most of the reported stress–strain curves of the CNT-based polymer composites illustrate loss of strain to failure.[3]

The nanocomposite dynamic mechanical properties as the function of the temperature

The effect of CNTs on the glass transition temperature of PP (T_g) and the temperature dependency of the dynamic storage modulus (G') was examined by DMA analysis of the PP/MWCNT nanocomposites in the broad temperature range from −60 to 160°C at fixed frequency 1 Hz. In Figures 7–9 the G' [Figs. 7(a), 8(a)], the relative storage modulus (G'/G'_{PP}) [Figs. 7(b), 8(b)] and loss factor (tan δ) (Fig. 9) are plotted as functions of the temperature for two series of the composites based on MWCNT(1)s and MWCNT(3)s depending on the MWCNT loading and surface modification. The nanocomposite relative storage moduli were calculated from data of Figures 7(a), 8(a) and visually demonstrate the change in the nanotube reinforcing effects with temperature.

The temperature dependency of tan δ for unfilled PP demonstrates two relaxation peaks: first at ca. 8°C and second less intense wider peak between 50 and 130°C (Fig. 9). The dominant relaxation at ca. 8°C is the glass–rubber relaxation of the amorphous rubber-like phase of PP. The wide high temperature peak on tan δ–T curve is frequently observed for the semicrystalline polymers and is associated with both intracrystalline relaxation (α-relaxation) and sliding of tied macromolecules within crystalline blocks of PP.[39] The presence of both MWCNT types does not practically effect on the T_g of the amorphous rubber-like phase PP. At the same time some widening the high temperature relaxation peak compared to that of neat PP occurs at the high MWCNT(1) and MWCNT(3) loadings (>3.5 vol %). Probable an additional amount of the polymer segments with a constrained molecular mobility appears, thus confirming interfacial interaction between the polymer and nanotubes.

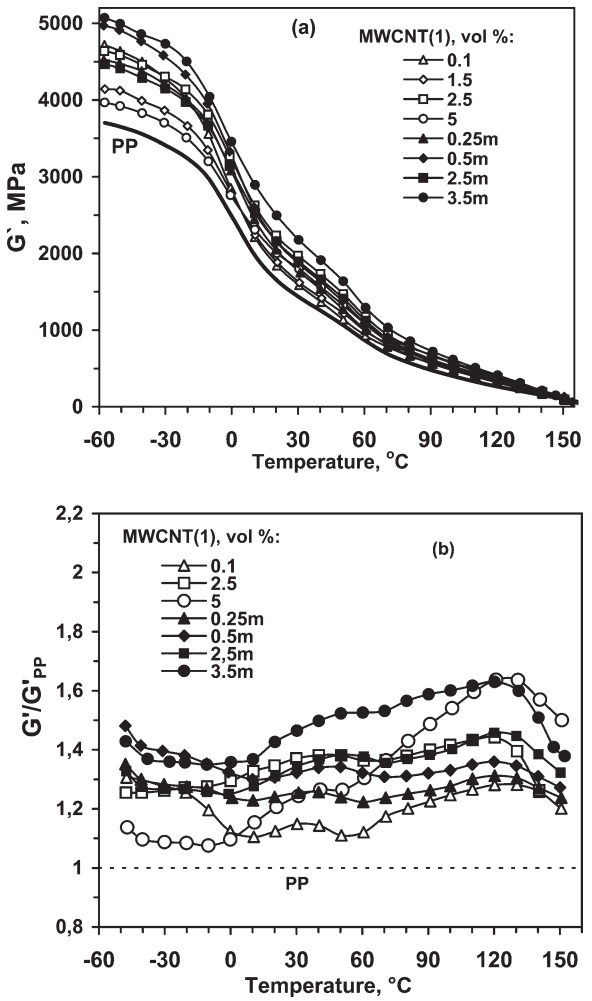

Figure 7 Storage moduli G′ (a) and relative storage moduli G'/G'_{PP} (b) for the MWCNT(1)-based composites as functions of temperature depending on the nanotube volume loading and surface modification.

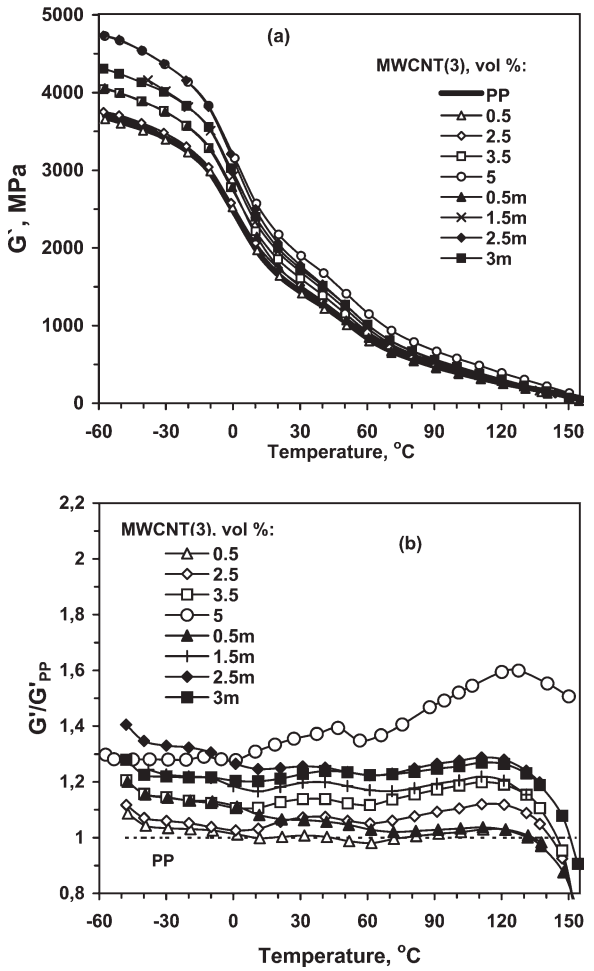

Figure 8 Storage moduli G′ (a) and relative storage moduli G'/G'_{PP} (b) for the MWCNT(3)-based composites as functions of temperature depending on the nanotube volume loading and surface modification.

The DMA data show that, in general, the composite storage modulus increases with increasing nanotube loading and with using the surface modified MWCNTs [Fig. 7(a,b)]. In the whole investigated temperature range the G'/G'_{PP} values for the composites based on MWCNT(1)s of the smaller diameter and greater intrinsic aspect ratio are lightly higher than those for MWCNT(3)-based composites [Fig. 8(a,b)]. For nanotube loading of 3.5–5 vol % the G'/G'_{PP} ratio is in the range of 1.4 and 1.35 for MWCNT(1)- and MWCNT(3)-based composites, respectively. The low experimental reinforcing effect measured by DMA for MWCNT(1)s, compared to expected one for nanotubes with high intrinsic L/d, agrees with mentioned earlier tension data, and is most likely caused by low $(L/d)_{eff}$ of thin flexible MWCNT(1)s.

The distinctive feature of composites with the highest loadings of both MWCNT(1)s and MWCNT(3)s is the visible tendency to rise in the

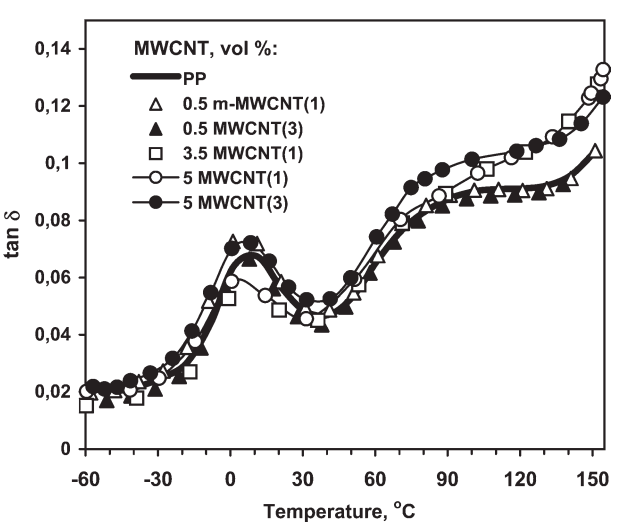

Figure 9 Loss factor tan δ as a function of temperature for the MWCNT composites depending on nanotube type, volume loading, and surface modification.

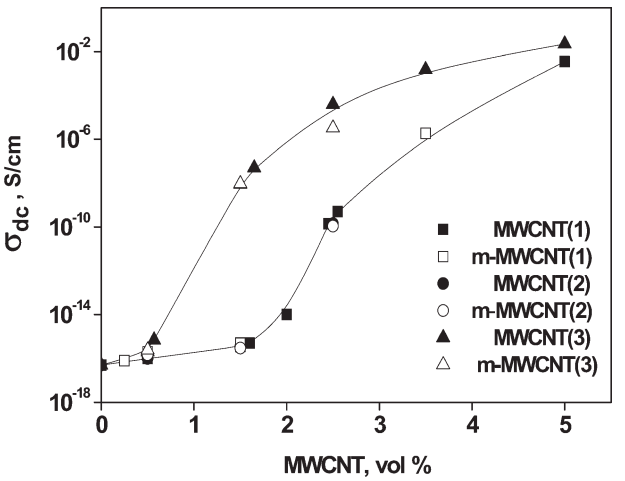

Figure 10 The electrical conductivity σ_{dc} of PP/carbon nanotubes composites versus the MWCNT volume loading depending on the MWCNT type.

reinforcing effect from 1.3–1.4 to 1.6 with increasing temperature above T_g. Similar increase in the G'/G'_{PP} ratio above T_g was reported previously for polymer composites based on CNTs,[21] isometric shape particles[39,40] and layered silicates.[41,42] The rise in reinforcing effect of rigid filler at $T > T_g$ can be partially attributed to several factors, such as change in the ratio of the modulus of the filler to that of the polymer above the glass transition,[39] as well as a restriction of the polymer relaxation dynamics caused by the physical entanglements between tied polymer molecules and nanotubes or formation the three dimensional nanotube network at critical filler content.[9] The accumulation of polymer chains with the constrained molecular mobility is confirmed by widening high temperature relaxation peaks on the tan δ–T dependencies with increasing of nanotube loading (Fig. 9). For understanding of these phenomena further research is required.

Electrical properties

Direct current conductivity σ_{dc}

The concentration dependencies of direct current conductivity σ_{dc} of PP composites with as-received and surface modified nanotubes for three MWCNT types are plotted in Figure 10. It can be seen that all PP/MWCNT composites exhibit a typical percolation behavior. The introduction of MWCNTs to PP increases the conductivity of the resulting composites by more than 10 orders of magnitude. According to the Figure 10 the percolation threshold value (Φ_c) for composites based on both MWCNT(1)s and MWCNT(2)s is 2.5 vol % and decreases to 1.5 vol % for composites with MWCNT(3)s. Data spread for samples with equal filler concentration was significantly larger than measurement error equals 5%. This spread was determined by percolation character of investigated systems and depended on the ratio Φ and Φ_c: 10%—in the case $\Phi \gg \Phi_c$, 20% if $\Phi \ll \Phi_c$, and 1–2 order of magnitude in the percolation region $\Phi \sim \Phi_c$.

The character of the σ_{dc} dependencies and the Φ_c values are determined in general by MWCNT type, whereas the surface modification does not practically effect on them. In Figure 11 the σ_{dc} concentration dependency for MWCNT(3)- based composites is compared with those for composites with traditional carbon fillers. As the conductivity of carbon multiwalled nanotubes is usually 10^2–10^3 S/cm, for comparison we used data for PP composites based on carbon fillers with close σ_{dc} values: (i) graphite EUZ-M (flake-shaped particles with L/d about 10 and $\sigma_{dc} = 10^3$ S/cm) and (ii) carbon black Vulcan XC-72 (chain structure clusters with L/d about 30 and $\sigma_{dc} = 10^2$ S/cm). As can be seen, the percolation threshold value for PP/MWCNT(3) composites is lower than those for composites based on graphite EUZ-M ($\Phi_c = 9.5$ vol %) and carbon black Vulcan XC-72 ($\Phi_c = 2.9$ vol %).

As a rule,[4,43] increasing the anisotropic conductive particle aspect ratio make it possible to reduce the filler loading necessary for the conductive network arrangement. The lower is the L/d, the higher should be Φ_c value. As follows from Figure 10, decreasing the Φ_c value with increasing the intrinsic nanotube L/d value takes place only in the case of two thick less clustering and curving MWCNT(2)s and MWCNT(3)s. On the other hand, the considerable rise in the MWCNT(1) intrinsic L/d up to 1000, by means of the decrease in nanotube diameter, leads to the increasing the percolation threshold for the MWCNT(1)-based composites. The rise in the Φ_c value required to form the conductive network is

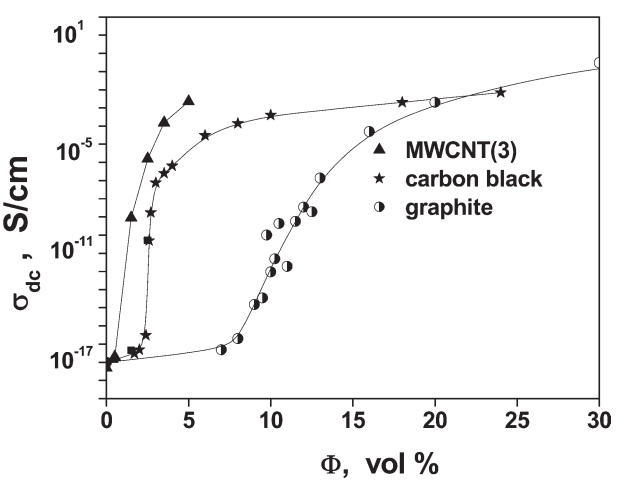

Figure 11 The electrical conductivity σ_{dc} versus carbon filler volume loading for the PP composites based on MWCNT(3)s, carbon black Vulcan XC-72 and graphite EUZ-M.

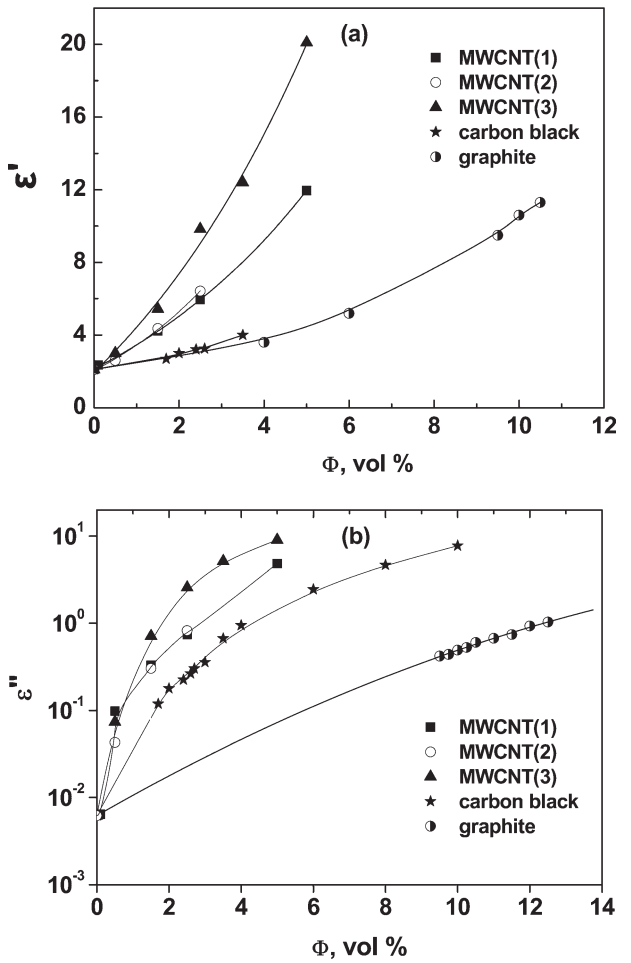

Figure 12 Dielectric permittivity ε′ (a) and losses ε″ (b) at frequency 10.5 GHz versus the carbon filler volume loading for PP composites based on three MWCNT types, carbon black Vulcan XC-72 and graphite EUZ-M.

most likely caused by the low $(L/d)_{\text{eff}}$ of MWCNT(1)s because the strong aggregation and entanglement of thin flexible nanotubes, as was shown earlier by TEM (Fig. 1 and Table II).

Dielectric properties

In Figure 12 the concentration dependences of dielectric permittivity ε′ (a) and losses ε″ (b) at frequency 10.5 GHz for the PP composites based on three MWCNT types, carbon black, and graphite are presented. The values of ε′ and ε″ for the composites based on MWCNT(3)s are higher than those for two other nanotube types practically in all concentration range. The dependences for the composites based on both MWCNT(1)s and MWCNT(2)s are very close to each other. The treatment of nanotube surface does not appreciably affect the ε′ and ε″, similar to dc-conductivity.

The composite dielectric properties in ultra-high frequency range mainly depend on filler conductivity, loading and particle effective aspect ratio $(L/d)_{\text{eff}}$. At equal filler loading and close conductivity, the higher $(L/d)_{\text{eff}}$ results in the higher dielectric permittivity and losses of composites. The flake-shaped particles of graphite have $(L/d)_{\text{eff}}$ value about 10. Carbon black particles form the chain structure clusters with $(L/d)_{\text{eff}}$ about 30. For MWCNT used the approximate $(L/d)_{\text{eff}}$ values within polymer matrix were estimated by correlation of dielectric properties of nanocomposites prepared with appropriate data for the graphite and carbon black based composites. The estimated $(L/d)_{\text{eff}}$ value are about 60 for MWCNT(3)s and about 35 for both the MWCNT(2)s and MWCNT(1)s.

Thus the analysis of the composite direct current conductivities and dielectric properties reveals that the long thick nanotubes MWCNT(3)s are characterized by highest effective aspect ratio in PP matrix. The estimated $(L/d)_{\text{eff}}$ value for the short thick MWCNT(2)s is close to the intrinsic L/d = 20–40 (Table I), i.e. their length is realized completely. The estimated $(L/d)_{\text{eff}}$ for the thin MWCNT(1)s is 30 times lower than intrinsic L/d and corresponds, apparently, to the effective aspect ratio of the agglomerates formed.

The frequency dependences of conductivity σ_{ac} (f) and permittivity

The frequency dependences of conductivity σ_{ac} (f) and permittivity for all PP/MWCNT composites were measured in the range 10^{-2}–10^{6} Hz. These dependences are similar for three types of nanotubes studied and are typical for other well known conductive fillers.[44] The frequency dependences $\sigma_{ac}(f)$ in the f range 10^{-2}–10^{6} Hz for PP/MWCNT(3)

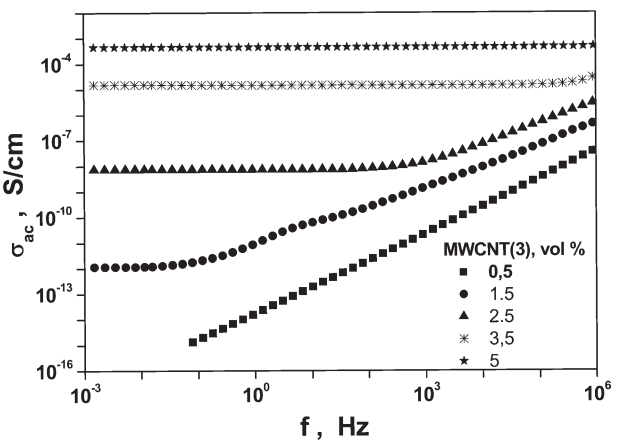

Figure 13 The frequency dependencies of ac-conductivity for PP/MWCNT(3) composites versus filler volume loading.

TABLE IV
The Coefficients of Transmission (*T*), Reflection (RD), and Absorption (*A*) of Electromagnetic waves, As Well As Reflection Coefficient of Sample on Metal Plate (RM) for Nanocomposites PP/MWCNT Depending on Nanotube Type and Volume Loading

Type of MWCNT	MWCNT (vol %)	*T* (%)	*RD* (%)	*A* (%)	*RM* (%)
MWCNT(1)	0	99.9	0.1	0	99.9
	0.25	91	7.1	1.9	90
	0.5	88.1	9	2.9	87.1
	1.5	63.1	21.6	15.3	57.5
	2.5	45.7	26.9	27.4	25.1
	3.5	23.4	49	27.6	27.5
	5	27.5	50.1	22.3	28
MWCNT(2)	0	99.9	0.1	0	99.9
	0.5	91	8.9	0.1	90
	1.5	72	16.6	11.4	70
	2.5	45	32	23	20
	3.5	32.4	47.9	19.7	49
MWCNT(3)	0	99.9	0.1	0	99.9
	1.5	62	23	15	60
	2.5	32.4	45.7	21.9	44.7
	3	27.5	47.9	24.6	39.8
	3.5	25.1	53.7	21.2	22.4
	5	14.5	48.9	36.6	6.6

$f = 37$ GHz, sample thickness is 0.45 mm.

composites are shown in Figure 13 as functions of the nanotube volume loading. The frequency dependencies of ε'_{ac} for PP/MWCNT(3) composites as functions of filler loading can be seen in Supporting Information (Figure SI2).

At $\Phi \ll \Phi_c$ the composite conductivity increases almost linearly with the frequency increase. Such character of σ_{ac} (f) dependency is typical for unfilled polymers. At $\Phi \gg \Phi_c$ the σ_{ac} of composites is independent from the frequency and coincides with σ_{dc} in the direction perpendicular to the sample plane. We can see that for composite with $\Phi \sim \Phi_c$ the conductivity is constant at low frequencies (low frequency plateau which is equal to σ_{dc}) and increases with rising frequency. The region of increase is linear in double logarithmic scale, that is $\sigma_{ac}(f) \sim f^n$. The value of n for composite with $\Phi = \Phi_c$ is so-called critical exponent x. This critical exponent is universal constant for percolation systems and depends only on the system dimensionality and structure of framework of infinite percolation cluster (Supporting Information, Fig. SI3). The critical exponent x for 3D samples with uniform distribution of filler particles can have the following values: $x = 0.73$ if framework of percolation cluster represents 3D irregular net (typical for composites with micron sized filler particles) or $x = 0.57$ if framework of percolation cluster represents fractal structure (typical for nanocomposites).[44] The nanotubes have micrometer size along the tube and nanometer size in two other directions. The question was—what is the structure of infinite cluster formed in the studied composites? As was determined from Figure 13 critical exponent x for composites PP/MWCNT(3) is equal to 0.75, which is close to the systems with 3D irregular net structure of infinite cluster.

Electrodynamical properties

The following electrodynamical properties in microwave region were measured to determine potential application of composites PP/MWCNT: transmission coefficient of electromagnetic waves through sample (T), reflection coefficient of electromagnetic waves from sample (RD), reflection coefficient from sample placed on metal plate (RM). Coefficient of absorption of electromagnetic waves in sample (A) was calculated using the formula: $A = 100\% - R - T$. The effect of volume loading and type of MWCNTs on the coefficient values at $f = 37$ GHz is given in Table IV. Data on the effect of frequency on the coefficient values for PP/MWCNT(3) and PP/MWCNT(1) nanocomposites with 5 vol % of loading are represented in Supporting Information (Table SI). As can be seen, the T and RM coefficients of the PP composites are reduced more intensively in the presence of the MWCNT(3)s compared to MWCNT(1)s and MWCNT(2)s.

For nanocomposite sample with 5 vol % of the MWCNT(3)s with optimal dimensions the dependencies of transmission coefficient T versus sample thickness (h) at different frequencies were calculated and plotted in Figure 14. It was calculated, that at the thickness of 2 mm only 1/300 of electromagnetic

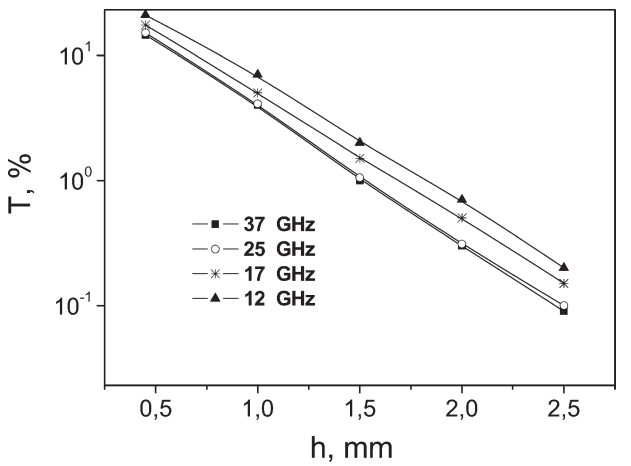

Figure 14 The electromagnetic waves transmission coefficient T versus sample thickness for PP/MWCNT(3) composites with 5 vol % nanotubes depending on frequency. Frequencies of electromagnetic waves are shown in the legend.

wave energy passes through the composite sample. For the 2 mm-thickness sample of the composite with 6 vol % of MWCNT(3)s the calculated T value falls to 1/2000.

The data obtained show that PP/MWCNT(3) composites can be used for development of multilayer absorbers of electromagnetic waves for personnel and equipment protection, for improvement of ecological situation around airports, cellular communications base stations, and so on. The composites with nanotube loading 4.5–5 vol % can be used as absorbing layers and with $\Phi = 2.5$–4.5 vol % - as matching layers. The PP/MWCNT(3) composites with $\Phi > 6$ vol % nanotube loading have dc-conductivity higher than 10^{-1} S/cm and can be used as thin and light screens for electromagnetic shielding.

CONCLUSIONS

Multiwalled nanotubes of small ($d < 10$ nm) and large ($d = 40$–60 nm) diameters have been used as filler to prepare the PP nanocomposites by melt mixing. The effects of the MWCNT diameters, intrinsic aspect ratios (L/d), and surface modification on the composite morphologies, mechanical reinforcement, and electrical properties have been clarified. The strong tendency of small diameter MWCNT(1)s with highest intrinsic value $L/d > 1000$ to bundle and cluster together in a polymer matrix was revealed by TEM and very cold neutrons scattering. The agglomerates of entangled structure form in the polymer composites with both as-received and surface modified MWCNT(1)s due to high flexibility of thin nanotubes, and their effective aspect ratio $(L/d)_{\text{eff}}$ is drastically reduced compared to high intrinsic L/d value. Both large diameter nanotubes with high $L/d \approx 300$ [MWCNT(3)s] and low $L/d \approx 20$–40 [MWCNT(2)s] are distributed within the polymer matrix mostly as isolated nonentangled nanotubes. The MWCNT(3)s exhibit the higher fraction of isolated nanotubes, the smaller mass-fractal dimension and higher degree of straightness within polymer matrix compared to those for small diameter thin nanotubes, indicating higher rigidity of thick MWCNTs.

The nanotubes of all types are heterogeneous nucleation sites for PP crystallization, but do not practically effect on the PP–matrix morphology. The small diameter MWCNT(1)s demonstrated the more noticeable nucleating effect due by their larger specific surface in spite of their tendency to agglomeration.

The DMA results showed an independence of the glass transition temperature of the PP amorphous rubber-like phase upon the MWCNT dimension and loading.

The both tensile testing and DMA analysis did not shown a considerable jump in the reinforcing effect of small diameter MWCNT(1)s in line with increasing their intrinsic L/d. The close maximal modulus enhancements equal to 1.35–1.40 near T_g and about 1.6 around 100°C were shown for nanocomposites containing 5 vol % of both thin MWCNT(1)s with intrinsic $L/d > 1000$ and thick MWCNT(3)s with intrinsic $L/d \approx 300$. The low reinforcing effect of small diameter MWCNT(1)s compared to expected one consequently to greater intrinsic L/d, is most likely caused by low effective aspect ratio $(L/d)_{\text{eff}}$ of thin flexible MWCNT(1)s within polymer matrix.

The study of composite electrical properties revealed that the character of the σ_{dc} dependencies and the percolation threshold values (Φ_c) are determined in general by MWCNT dimension, whereas the surface modification does not practically effect on them. The nanocomposites based on the long large diameter MWCNT(3)s showed the lowest percolation threshold equal to 1.5 vol % loading, highest dielectric and electromagnetic waves shielding properties. The higher Φ_c value observed for composites based on thin MWCNT(1)s with higher intrinsic L/d was explained by drop of $(L/d)_{\text{eff}}$ caused by clustering and entanglement of thin nanotubes.

The study of both electrical and mechanical properties of PP/MWCNT composites showed maximal efficiency for the large diameter MWCNT(3)s with most optimal structure parameters. The increase in the MWCNT(1) aspect ratio by means of diameter decreasing reduces their efficiency due to the high flexibility and entanglement of thin nanotubes, leading to $(L/d)_{\text{eff}}$ decrease. Thus, the improvement in the dispersion state and straightness of multiwelled CNTs in polymer melt as well as the enhancement of their efficiency as reinforcing and conductive

nanosized filler can be achieved by choice of the optimal diameter and length of MWCNTs.

Authors thank Dr. Sergey S. Abramchuk from Moscow State University for the great assistance in transmission electron microscopy analysis.

References

1. Iijima, S. Nature 1991, 354, 56.
2. Coleman, J. N.; Khan, U.; Blau, W. J.; Gun'ko, Y. K. Carbon 2006, 44, 1624.
3. Du, J.-H.; Bai, J.; Cheng, H.-M. Express Polym Lett 2007, 1, 253.
4. Bauhofer, W.; Kovacs, J. Z. Compos Sci Technol 2009, 69, 1486.
5. Al-Saleh, M. H.; Sundararaj, Ut. Carbon 2009, 47, 2.
6. Moniruzzaman, M.; Winey, K. I. Macromolecules 2006, 39, 5194.
7. Abdalla, M.; Dean, D.; Robinson, P.; Nyairo, E. Polymer 2008, 49, 3310.
8. Sureeyatanapas, P.; Young, R. J. Compos Sci Technol 2009, 69, 1547.
9. Du, F.; Scogna, R. C.; Zhou, W.; Brand, S.; Fischer, J. E.; Winey, K. I. Macromolecules 2004, 37, 9048.
10. Krause, B.; Pötschke, P.; Häußler, L. Compos Sci Technol 2009, 69, 1505.
11. Lee, S. H.; Kim, J. H.; Kim, K. W.; Youn, J. R.; Choi, S. H.; Kim, S. Y. Polym Int 2009, 58, 354.
12. Pegel, S.; Pötschke, P.; Petzold, G.; Alig, I.; Dudkin, S. M.; Lellinger, D. Polymer 2008, 49, 974.
13. Chen, G.-X.; Kim, H.-S.; Park, B. H.; Yoon, J.-S. Polymer 2006, 47, 4760.
14. Grossiord, N.; Kivit, P. J. J.; Loos, J.; Meuldijk, J.; Kyrylyuk, A. V.; van der Schoot, P.; Koning, C. E. Polymer 2008, 49, 2866.
15. Tong, X.; Liu, C.; Cheng, H. M.; Zhao, H. C.; Yang, F.; Zhang, X. Q. J Appl Polym Sci 2004, 92, 3697.
16. Lozano, K.; Yang, S. Y.; Jones, R. E. Carbon 2004, 42, 2329.
17. Kanagaraj, S.; Varanda, F. R.; Zhil'tsova, T. V.; Mónica, S. A.; Simões, O.; Simões, J. A. O. Compos Sci Technol 2007, 67, 3071.
18. Zhou, Z.; Wang, S.; Zhang, Y.; Zhang, Y. J Appl Polym Sci 2006, 102, 4823.
19. Bao, H.-D.; Guo, Z.-X.; Yu, J. Polymer 2008, 49, 3826.
20. Wu, D.; Sun, Y.; Wu, L.; Zhang, M. J Appl Polym Sci 2008, 108, 1506.
21. Lee, G.-W.; Jagannathan, S.; Chae, H. G.; Minus, M. L.; Kumar, S. Polymer 2008, 49, 1831.
22. Manchado, L.; Valentini, L.; Biagiotti, J.; Kenny, J. M. Carbon 2005, 43, 1499.
23. Schaefer, D. W.; Justice, R. S. Macromolecules 2007, 40, 8501.
24. Cooper, C. A.; Ravich, D.; Lips, D.; Mayer, J. J.; Wagner, H. D. Compos Sci Technol 2002, 62, 1105.
25. Bai, J. B.; Allaoui, A. Compos A 2003, 34, 689.
26. Kovacs, J. Z.; Andresen, K.; Pauls, J. R.; Pardo, G. C.; Schossig, M.; Schulte, K.; Bauhofer, W. Carbon 2007, 45, 1279.
27. Chen, J.; Hamon, M. A.; Hu, H.; Chen, Y. S.; Rao, A. M.; Eklund, P. C.; Haddon, R. C. Science 1998, 282, 95.
28. Mickelson, E. T.; Huffman, C. B.; Rinzler, A. G.; Smalley, R. E.; Hauge, R. H. Chem Phys Lett 1998, 296, 188.
29. Khabashesku, V. N.; Billups, W. E.; Margrave, J. L. Acc Chem Res 2002, 35, 1087.
30. Lee, R. S.; Kim, H. J.; Fischer, J. E.; Thess, A.; Smalley, R. E. Nature 1997, 388, 255.
31. Grinev, V. G.; Kuznetsov, S. P.; Meshkov, I. V.; Optov, V. G.; Perekrestenko, A. D.; Raspopov, L. N.; Shelagin, A. V. Polym Sci 1993, 35, 197.
32. Wunderlich, B. Macromolecular Physics; Academic Press: New York, 1976; Vol II.
33. Agilent Technologies Application Note. PN 5989-2589E "Basics of Measuring the Dielectric Properties of Materials", 2006; Available at http://cp.literature.agilent.com/litweb/pdf/5989-2589EN.pdf (accessed June, 2006).
34. Nyden, M. R.; Stoliarov, S. I. Polymer 2008, 49, 635.
35. Xu, D.; Wang, Z. Polymer 2008, 49, 330.
36. Agarwal, B. D.; Broutman, L. G. Analysis and Performance of Fiber Composites; Wiley: New York, 1980.
37. Mallick, P. K. Fiber-Reinforced Composites; Marcel Dekker: New York, 1993.
38. Nicolais, L.; Narkis, M. Polym Eng Sci 1971, 11, 1971.
39. Nilsen, L. E. Mechanical Properties of Polymers and Composites; Marcel Dekker: New York, 1974.
40. Dubnikova, I. L.; Nizhegorodtseva, E. I.; Lomakin, S. M.; Krasheninnikov, V. G.; Gorenberg, A. Ya; Kuleznev, V. N. Polym Sci Ser A 2008, 50, 1214.
41. Ray, S. S.; Okamoto, M. Prog Polym Sci 2003, 28, 1539.
42. Dubnikova, I. L.; Berezina, S. M.; Korolev, Y.uM.; Kim, G.-M.; Lomakin, S. M. J Appl Polym Sci 2007, 105, 3836.
43. Shevchenko, V. G.; Ponomarenko, A. T.; Klason, C.; Tchmutin, I. A.; Ryvkina, N. G. Electromagnetics 1997, 17, 157.
44. Watts, P. C. P.; Fearon, P. K.; Hsu, W. K.; Billingham, N. C.; Kroto, H. W.; Walton, D. R. M. J Mater Chem 2003, 13, 491.